Nanoscale

Accepted Manuscript

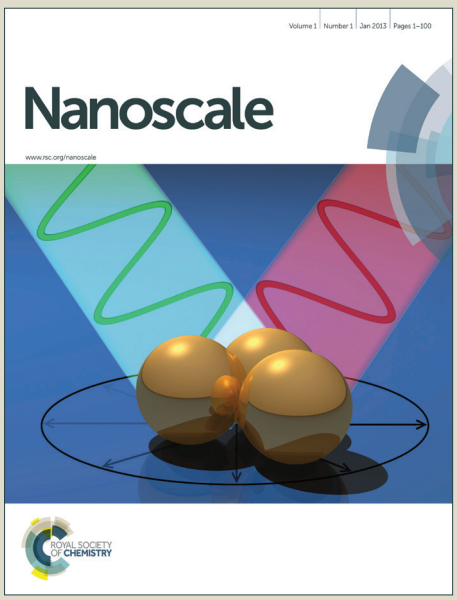

ROYAL SOCIETY OF CHEMISTRY

www.rsc.org/nanoscale

Nanoscale

RSCPublishing

COMMUNICATION

Quantum Dots on Vertically Aligned Gold Nanorod Monolayer: Plasmon Enhanced Fluorescence

Cite this: DOI: 10.1039/xoxxoooooox

Received ooth January 2012,
Accepted ooth January 2012

DOI: 10.1039/xoxxoooooox

www.rsc.org/

Bo Peng,[a] Zhenpeng Li,[a] Evren Mutlugun,[c] Pedro Ludwig Hernández Martínez,[c] Dehui Li,[a] Qing Zhang,[a] Yuan Gao,[a,c] Hilmi Volkan Demir,*[a,c,d] and Qihua Xiong*[a,b]

CTAB-coated Au nanorods were directly self-assembled into a vertically aligned monolayer with highly uniform hot spots through a simple but robust approach. By coupling with CdSe/ZnS quantum dots, a maximum enhancement of 10.4 is achieved due to: the increased excitation transition rate, radiative rate, and coupling efficiency of emission to the far field.

Plasmonics exhibits the potential to manipulate optics at the sub-wavelength scale, promising exciting applications including negative refractive index media and metamaterials.[1-5] The self-assembly of monodisperse nanoparticles into ordered structures is an effective approach for designing plasmonics.[6-9] Spherical Au nanoparticles have been manipulated to generate a diverse selection of plasmonic topologies such as superlattice sheets,[10, 11] chain networks,[12] and chiral pyramidal structures.[13] However, ordered assemblies of anisotropic nanostructures, such as Au nanorods, is still very challenging, because the anisotropic shape results in various assembling behaviours. By the Langmuir–Blodgett technique,[14, 15] hydrophobic polymer-modified Au nanorods were self-assembled into monolayer sheets consisting of random horizontal and vertical Au nanorods at the air-water interface.[16] Recently, based on the coffee-ring effect, the evaporation-induced self-assembly have been developed.[17] During the evaporation of solvent, a flow from the inner region replenishes the liquid that is evaporated at the edge. As a result, nanorods are transferred to the droplet edge and self-assembled into ordered multilayer parallel arrays.[18, 19] Meanwhile, a near-equilibrium status is also formed at the internal region of the drying droplet, which contributes to the self-assembly of free anisotropic nanostructures to their lowest energy state in solution. Few previous studies have reported the formation of multilayer vertical arrays by decreasing the electrostatic repulsive force via modifying Au nanorods with weak polar ligands instead of cetyltrimethyl-ammonium bromide (CTAB).[20, 21] Until recently, there are only few reports on the directional self-assembly of CTAB-stabilized Au nanorods into vertically aligned multilayer arrays.[22, 23] Recently, our group has shown that it is possible to directly self-assemble CTAB-coated Au nanorods into highly organized vertical monolayer arrays by synergistically controlling the electrostatic repulsive force and van der Waals attractive force.[24]

In the past decade, plasmonics has been proven to enhance or quench fluorescence as a function of distance between the surface plasmon and fluorophores.[25-30] The previous reports focused their research on the interactions between fluorophores and single Au nanoparticle,[31] single silver nanoprisms,[32] and Au disk or hole arrays.[33] However, a handful work reported the resonant energy transfer based on the metallic colloid arrays as surface plasmonic system.[34, 35] Moreover, many colloid substrates suffer from poor reproducibility of "hot spots". Herein, we demonstrate a simple yet robust approach to directionally assemble CTAB-coated Au nanorods into a vertically aligned monolayer and investigate the energy transfer between plasmonic array and monolayer CdSe/ZnS quantum dots (QDs). The vertically aligned Au nanorod monolayer exhibit a strong, reproducible, and highly homogeneous distribution of hot spots. Our experiments show that the Au nanorods with the aspect ratio from 2.1 to 3.2 can be self-assembled into a vertically aligned monolayer and the electrostatic force and van der Waals force predominate in the self-assembly. The SiO_2 films were coated on the vertically aligned Au nanorod monolayer by sputter deposition as a spacer to tune the distance between plasmonic monolayer and QDs. A distinct plasmonic enhancement property was uncovered and a maximum fluorescence enhancement of 10.4 was achieved at a 20 nm SiO_2 spacer. Fluorescence-lifetime imaging microscopy (FLIM) was used to measure the lifetime of QDs, which decreased from ~4.1 ns to minimum, ~0.9 ns, due to the increased radiative decay rate. Therefore, the plasmonic monolayer arrays, due to its enhanced optical density of states, can serve as 2D optical

materials such as directionality controller, light enhancers, colour filters, and ultrasensitive SERS sensors.[36-38]

Based on the evaporation-induced strategy, CTAB-coated Au nanorods with the aspect ratio of ~2.7, which were synthesized by seeded growth method,[39] were self-assembled into a vertically aligned monolayer on Si substrates when the Debye length was 3.0 nm (Fig. 1a). The Au nanorods in the monolayer are aligned to a hexagonal close-packed structure. The inset in Fig. 1a shows the three-dimensional schematic diagram of the arrays. The interior gap distance between two adjacent Au nanorods is ~7.7 nm. Fig. 1b exhibits the monolayer structure in a vivid fashion. Surprisingly, the vertically aligned hexagonal Au nanorod bi-layer was formed in the case that the Debye length decreased to 1.3 nm by adding NaCl (Fig. 1c) and the interior gap distance is ~3.4 nm, which corresponds to the length of a CTAB bi-layer.[17, 40] Our approach can be extended to other Au nanorods with different aspect ratio. Fig. 1d shows the absorption spectra of different Au nanorods. The longitudinal plasmon bands are 656, 680, 717, 755 and 780 nm, where the aspect ratio are 2.1, 2.3, 2.7, 2.9 and 3.2, respectively. And the diameters of the corresponding Au nanorods are ~45.4, 42.6, 39.8, 32.3 and 27.3 nm, while the lengths are ~94.2, 96, 100.5, 94.1, and 88.2 nm, respectively.

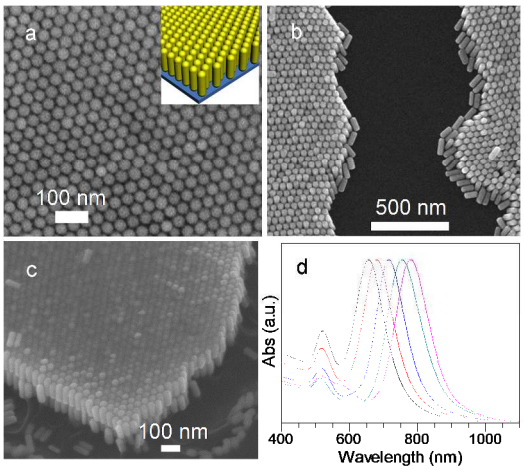

Fig. 1 SEM image of vertically aligned Au nanorod monolayer: (a) top view, (b) view from the edge. The insets in (a) show the schematic picture of vertically aligned self-assembled Au nanorod monolayer. (c) The side-view SEM image of vertically aligned hexagonal Au nanorod bi-layer. (d) The absorption spectra of Au nanorod aqueous solution. The longitudinal plasmon bands are 656, 680, 717, 755 and 780 nm, respectively.

During the self-assembly of Au nanorods, there are three forces: van der Waals force, depletion force and electrostatic force, whose energy is defined by E_{Vdw}, E_{dep}, E_{ele}, respectively. Van der Waals and depletion force are the attractive forces and electrostatic force is the repulsive force. The attractive forces push Au nanorods to approach together, where the repulsive forces make the nanorods move away from each other. Therefore, the synergy between the repulsive force and attractive force ensures the alignment of Au nanorods at the equilibrium status, rather than random aggregation. We calculated E_{Vdw}, E_{dep} and E_{ele} for five kinds of Au nanorods with 656, 680, 717, 755 and 780 nm plasmon band as a function of edge-to-edge gap size in the case that the Debye length was 3.0 nm. E_{Vdw} and E_{dep} can be obtained by the previous reports.[20, 41] For all Au nanorods, E_{Vdw} is much larger than E_{dep}. Both E_{Vdw} and E_{dep} increase as the gap size decrease (Fig. 2a). But E_{Vdw} and E_{dep} decrease as plasmon band increase from 656 nm to 780 nm. To calculate E_{ele} between two adjacent Au nanorods, the Derjaguin's approximation is used.[42] We assume the Au nanorod consists of many slices of parallel thin plates, which contribute to E_{ele}.[40] Fig. 2c shows that E_{ele} decreases with the increasing gap size and also decreases as the plasmon band of Au nanorods increase from 656 to 780 nm. We define the total interaction energy by $E_{Total} = E_{Vdw} + E_{dep} + E_{ele}$, which first decreases to a minimum and then increases as the gap size increases. However, for all Au nanorods with different plasmon bands, the total energy is minimized at 7.5 nm gap size, which indicates that all Au nanorods can be self-assembled into a vertically aligned monolayer. When the Debye length is decreased to 1.3 nm by adding NaCl, the calculated minimum E_{Total} is achieved at a gap size of 3.9 nm. However, the lowest limit we can achieve in aligned Au nanorod monolayer is ~6.7 nm. Therefore, vertically aligned Au nanorod bi-layer is formed to achieve the lowest energy state. In our experiments, the edge-to-edge gap size of bi-layer arrays is ~3.4 nm in the case that the Debye length is 1.3 nm. We suggest that the CTAB molecules are inter-digitated when they approach to touch each other, which leads to strong depletion force.[17] Therefore, the experimental gap size is a little smaller than the calculated data.

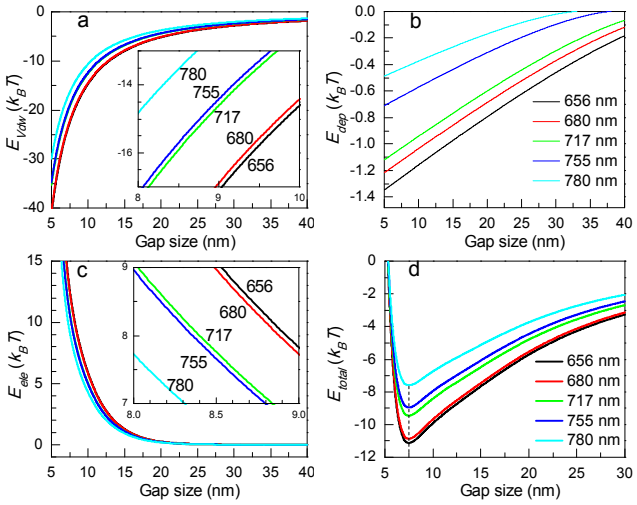

Fig. 2 Interaction free energy as a function of gap size in the case that the Debye length k^{-1} is 3 nm: (a) van der Waals force, E_{Vdw}, (b) depletion force, E_{dep}, (c) electrostatic repulsive force, E_{ele}, (d) total interaction energy, defined by $E_{Total} = E_{Vdw} + E_{dep} + E_{ele}$.

We focused on the monolayer arrays consisting of Au nanorods with a longitudinal plasmon band at 717 nm and investigated the energy transfer between plasmonic array and monolayer CdSe/ZnS QDs. Sputtered SiO_2 layer was used as a spacer to control the distance between plasmonic monolayer and QDs (Figure 3a). 10 μL CdSe/ZnS QDs hexane dispersion was drop-cast onto the surface of acetonitrile in a Teflon well (~ 2 × 2 × 2 cm^3).[6] A monolayer quantum dot (QD) self-assembled film was formed within 5 s and then transferred onto the vertically aligned Au nanorod monolayer (Figure 3b). The absorption peak of vertically aligned monolayer consisting of Au nanorod with 717 nm plasmon band is ~610 nm checked by CRAIC 20 microspectrophotometer (Figure 3c). The polarization of white light was parallel to the interparticle distance. Therefore, the transverse plasmon modes interact attractively and these underwent a red shift from ~520 to ~610 nm.[43] The photoluminescence (PL) of CdSe/ZnS QD monolayer with and without plasmonic coupling was measured by a home-built system. A 532 nm laser was used as the excitation, whose polarization direction was along the side of Au nanorod hexagon in the vertically aligned monolayer. Figure 3d shows the room-temperature steady-state PL spectra of CdSe/ZnS QD monolayer on Si substrates and the vertically aligned Au nanorod monolayer, respectively. The PL peak

is at ~614 nm, which is close to the absorption peak of Au rod arrays. Therefore, a maximum coupling between PL and the scattering of vertically aligned Au nanorod monolayer can be achieved, which influences the enhancement of QD emission.[44] A pronounced SiO_2 spacer dependence is spotted from Figure 3c. We evaluate the enhancement factor (EF) using $EF = I/I_0$, where I and I_0 are the PL intensities of CdSe/ZnS QD monolayer with and without the vertically aligned Au nanorod monolayer, respectively. The PL intensities are extracted and EF is plotted versus SiO_2 spacer in Figure 3e. When the SiO_2 spacer thickness is ~5 nm, the PL of the QD monolayer on vertically aligned Au nanorod monolayer is quenched.[22] When we systematically change the separation between QDs and the plasmonic array, we have clearly observed the distance dependent PL enhancement. The PL intensity with plasmonic coupling at a 10 nm SiO_2 spacer is slightly larger than that of QD monolayer without plasmonic coupling. When the SiO_2 spacer is further increased to ~50 nm, the PL intensity of QD monolayer on the vertically aligned Au nanorod monolayer is comparable to the PL signal of the QD monolayer on Si substrates within the experimental error, which indicates that the plasmonic coupling has barely any effect to the PL when the spacer is larger than ~50 nm. In our experiments, PL exhibits a local maximum at ~20 nm SiO_2 spacer as also in agreement with the previous reports.[35, 45] Generally speaking, the incident light is confined into a small spatial space by the surface plasmon, resulting in a strong local electromagnetic fields, $|E|$. The coupling of the excited dipole with plasmons not only has a great effect on both nonradiative and radiative mode of the transition dipole, but also increases the absorption of incident light.[46] The competition of nonradiative and radiative mode determines the PL quenching and enhancement. In the case of PL quenching, the nonradiative energy transfer from fluorophores to plasmonic monolayer predominates. Both the small distance and the large spectral overlap between PL spectra and plasmon band are great of benefit to a fast nonradiative energy transfer from the excited dipole

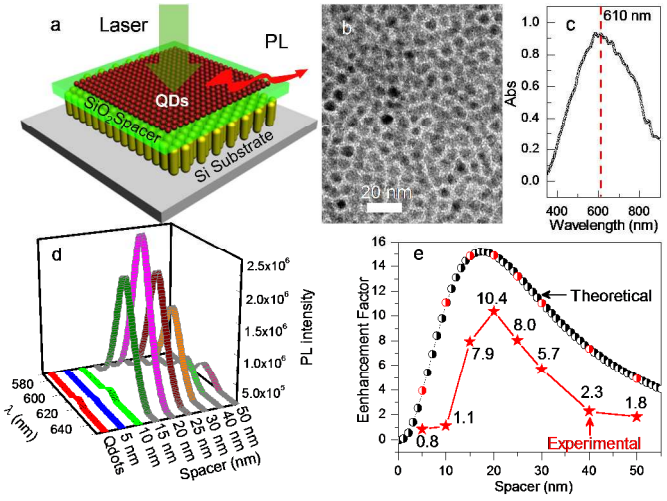

Fig. 3 (a) Schematic picture of the coupling of vertically aligned Au nanorod monolayer and CdSe/ZnS QDs monolayer films. SiO_2 layer is used as a spacer to control the distance between plasmonic monolayer and QDs. (b) TEM image of monolayer films of CdSe/ZnS QDs (QDs) with PL emission at 614 nm. (c) Normalized absorption spectrum of vertically aligned monolayer consisting of Au nanorods with 717 nm plasmon band. (d) Photoluminescence spectra of CdSe/ZnS QDs monolayer films on vertically aligned Au nanorod monolayer. The silica spacer thickness is 5, 10, 15, 20, 25, 30, 40, and 50 nm, respectively. Non-monotonous behaviour is noticed. (e) Plot of calculation (black line + circle, the red circle show the theoretical data at the experimental spacer thickness) and experimental (red line + star) enhancement factor as a function of the silica spacer thickness.

to the plasmon. In the case of the PL enhancement, first of all, the absorption increases due to the increase of $|E|$, $\gamma_{exc} \propto |p \cdot E|^2$, where p is the transition dipole moment of the fluorophores.[25] Second, the radiative rate is enhanced significantly due to Purcell effect.[29, 44, 47, 48] Because the radiative rate is related to $|E|^2$, $r_{rad}^{sp} \propto |E|^2 r_{rad}^0$, where the radiative decay rate with and without plasmonic coupling are r_{rad}^{sp} and r_{rad}^0.[33] Therefore, the enhancement factors are large enough to exhibit the increase of PL intensity.[31, 35, 46] In our case, the plasmon resonance frequency (~610 nm) corresponds to the emission frequency (~614 nm) of CdSe/ZnS QDs. Therefore, the coupling of QD emission to the far field is increased by the scattering of Au nanorod monolayer arrays, which also induces PL enhancement.[44]

To theoretically estimate the enhancement factor, we consider two main assumptions. First, we calculate the normalized rate of energy dissipation due to a radiative dipole on top of a metallic surface. Second, we estimate the electric field enhancement due the surface plasmon of the metallic nanorod where the cylinder surface plasmon is approximated to a disk. The total effective electric field of one unit in the vertically aligned monolayer is assumed to be 6 time stronger than one disk because the Au nanorod are aligned in a hexagonal close packed structure. Therefore, the intensity enhancement factor is defined as

$$\eta(\mathbf{r},\mathbf{r}',\omega_{excitation},\omega_{emission}) = A(\mathbf{r},\omega_{excitation})\left(\frac{P(\mathbf{r}',\omega_{emission})}{P_0(\mathbf{r}',\omega_{emission})}\right)^{-1}$$

where P/P_0 is the normalized rate of energy dissipation of a radiative dipole defined as[49, 50]

$$\frac{P}{P_0} = 1 + \frac{1}{2}\mathrm{Re}\left(\int_0^\infty \frac{s^3 ds}{\sqrt{1-s^2}} r^{(p)}(s)\exp\left[2ik_1\left(\sqrt{1-s^2}\right)h\right]\right) +$$

$$\frac{1}{2}\mathrm{Re}\left(\int_0^\infty \frac{s ds}{\sqrt{1-s^2}}\left[r^{(s)}(s) - \left(1-s^2\right)r^{(p)}(s)\right]\exp\left[2ik_1\left(\sqrt{1-s^2}\right)h\right]\right)$$

where $r^{(s)}(s)$ and $r^{(p)}(s)$ are the reflection coefficients for s- and p-polarized waves, respectively, defined as

$$r^{(s)}(s) = \frac{k_1\sqrt{1-s^2} - \sqrt{k_2^2 - s^2k_1^2}}{k_1\sqrt{1-s^2} + \sqrt{k_2^2 - s^2k_1^2}}$$

$$r^{(p)}(s) = \frac{\varepsilon_2 k_1\sqrt{1-s^2} - \varepsilon_1\sqrt{k_2^2 - s^2k_1^2}}{\varepsilon_2 k_1\sqrt{1-s^2} + \varepsilon_1\sqrt{k_2^2 - s^2k_1^2}}$$

where ε_i and k_i are the dielectric constant and wave vector of the medium 1 (SiO_2 spacer) and 2 (Au rod). And the electric field enhancement factor due to the presence of metallic nanostructure is defined as[51]

$$A(\mathbf{r},\omega)=\frac{\int_{V_{QD}}\left|E_{Metal}(\mathbf{r},\omega)\right|^2 dV}{\int_{V_{QD}}\left|E_0(\mathbf{r},\omega)\right|^2 dV}$$

where $E_0(\mathbf{r},\omega)$ and $E_{Metal}(\mathbf{r},\omega)$ are the electric field without and with metallic nanostructure, respectively. The electric field for the cylinder with radius "a" is

$$\mathbf{E}(\mathbf{r})=\mathbf{E_0}\begin{cases}\dfrac{1}{1+\left(\dfrac{z}{a}\right)^2}\hat{z} & \rho=0;\ z>0\\ \displaystyle\int_0^1\left(\frac{1}{\sqrt{1-\rho_0^2}}\right)\left[\frac{\left(\dfrac{\rho}{a}-\rho_0\right)\hat{\rho}+\dfrac{z}{a}\hat{z}}{\left[\left(\dfrac{\rho}{a}-\rho_0\right)^2+\left(\dfrac{z}{a}\right)^2\right]^{\frac{3}{2}}}\right]\rho_0 d\rho_0 & \rho>0;\ z>0\end{cases}$$

where ρ is the radial component of the electric field perpendicular to the cylinder axis. z is the z component of the electric field parallel to the cylinder axis. As shown in Figure 3e, the numerical calculation results are in good agreement with our experimental data.

To understand the coupling of plasmonic monolayer and QDs, fluorescence-lifetime imaging microscopy was used to obtain time-resolved fluorescence spectroscopy, which is critically dependent on the distance between the plasmonic monolayer and QDs. Figure 4a shows the microscopic image of the vertically aligned Au nanorod monolayer (yellow color) coated by CdSe/ZnS QD monolayer film. The SiO_2 spacer is 10 nm. From the crack band of QD monolayer films, it clearly shows that the QD monolayer films are darker than Si substrates and cover on the vertically aligned Au nanorod monolayer. Figure 4b shows the FLIM image of QD monolayer corresponding to Figure 4a. The crack band of QD monolayer film is vivid. The lifetime of CdSe/ZnS QD monolayer on vertically aligned Au nanorod monolayer is much shorter than that on Si substrates, which indicates that the lifetime of QDs decreases due to plasmonic interaction. Figure 4c shows time-resolved PL spectra of CdSe/ZnS QDs. The SiO_2 spacer thicknesses are 0, 5, 10, 15, 20, 25, 30, 40 and 50 nm, respectively. All the time-resolved PL decay curve can be well fitted as a bi-exponential function, $I(t)=A_1\exp(-t/\tau_1)+A_2\exp(-t/\tau_2)$, with two time constants: a fast decay (τ_1) accompanied by a long-living emission (τ_2), where $I(t)$ is the PL intensity.[52, 53] The results are consistent with previous studies. The fast decay τ_1 is associated with recombination of carriers from the delocalized states in the core region, where the slow decay τ_2 originates from recombination of carriers from the localized states at the hetero-interface.[54, 55] The average lifetime is defined by $\tau=\tau_1\times a_1+\tau_2\times a_2$, where a_1 and a_2 are the fraction of τ_1 and τ_2, respectively. For CdSe/ZnS QDs on Si substrates, the lifetime is τ = 4.1±0.1 ns (τ_1 = 2.3±0.3 ns and τ_2 = 10.3±2.1 ns). Figure 4d shows the lifetime τ as a function of SiO_2 spacer thickness. The lifetime was obtained by measurement and statistical analysis of many CdSe/ZnS QD monolayer on the vertically aligned Au nanorod monolayer (>10). The decay lifetimes τ are 2.4±0.14, 2.0±0.2, 1.8±0.15, 0.9±0.1, 1.9±0.25, 2.6±0.16, 3.5±0.21, and 3.7±0.2 ns in the case that SiO_2 spacer thickness is 0, 5, 10, 15, 20, 25, 30, 40 and 50 nm, respectively. The lifetime first achieves a minimum at a 20 nm spacer and then increase, which is corresponding to the PL enhancement results, where the enhancement of 10.4 times is maximized at a 20 nm spacer. It is important to note that the trends of τ_1 and τ_2 as a function of silica spacer thickness are same with τ, as shown in the insets in Figure 4d. Both τ_1 and τ_2 are minimized in the case of a 20 nm silica spacer. The decrease of life time is corresponding to the pronounced enhancement of PL. Therefore, the increased radiative rate is large enough and contributes to the PL enhancement, although plasmon coupling enhances both radiative and nonradiative rate.[32, 46] Generally speaking, three factors determine the overall PL enhancement: increased transition rate of electrons, increased radiative rate due to the coupling of the excitons with plasmons, and enhanced coupling efficiency of the fluorescence emission to the far field.[44] When CdSe/ZnS QDs are excited by the incident photons, the electrons in the valence band transfer into conduction band. The transition rate can be enhanced by surface plasmon, because the photon absorption of QDs is increased by plasmonic coupling.[25] Meanwhile, the vertically aligned Au nanorod monolayer reflects the incident photons to excite CdSe/ZnS QDs again, which also contribute to the enhancement of transition rate.[34] When exciton recombination induces PL emission, a new modified radiative decay rate is induced due to plasmonic coupling, r_{rad}^{new}. Therefore, the radiative decay rate is accelerated, $r_{rad}^{sp}=r_{rad}^{0}+r_{rad}^{new}$, where r_{rad}^{sp} and r_{rad}^{0} are the radiative decay rate with and without plasmonic coupling, respectively.[34] Furthermore, the correspondence between plasmon resonance frequency (~610 nm) and emission frequency (~614 nm) enhances the coupling efficiency of emission to the far field. Therefore, the PL of CdSe/ZnS QDs is enhanced by plasmons. Therefore, we suggest that the increased excitation transition rate,

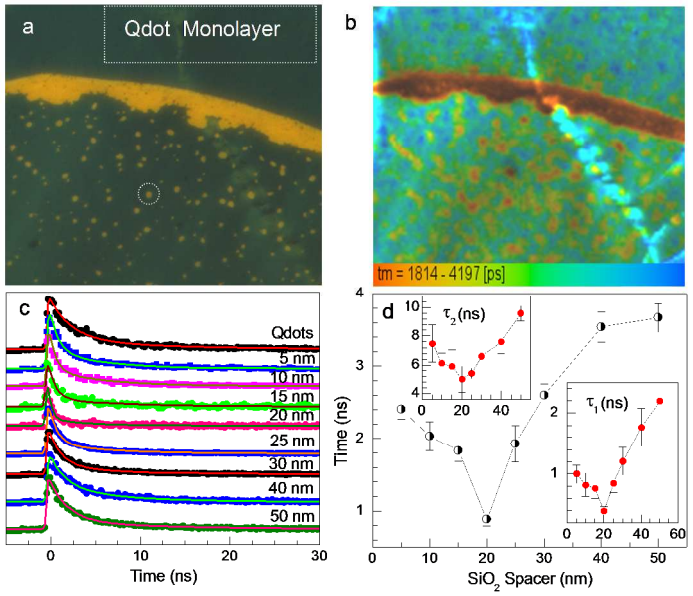

Fig. 4 (a) Optical microscopy image of vertically aligned Au nanorod monolayer covered by CdSe/ZnS QD monolayer films. The SiO_2 spacer is 10 nm. (b) Fluorescence-lifetime microscopy image of CdSe/ZnS QD monolayer films corresponding to (a). The corresponding vertically aligned Au nanorod monolayer covered by QD monolayer in (a) are shown in the white dotted circles. The bare CdSe/ZnS QD monolayer is outside of the golden yellow in (a). The lifetime of CdSe/ZnS QDs is shortened vividly on the vertically aligned Au nanorod monolayer. (c) Time-resolved fluorescence spectra of CdSe/ZnS QD monolayer films on vertically aligned Au nanorod monolayer. The silica spacer thickness is 5, 10, 15, 20, 25, 30, 40, and 50 nm, respectively. The solid lines are fits to the data using an exponential decay function as described in the text. (d) The average lifetime τ as a numerical function of the silica spacer thickness. The lifetime was obtained by measurement and statistical analysis of (b). The insets show τ_1 and τ_2 *versus* the silica spacer thickness, respectively.

radiative rate of excition recombination for emission, and coupling efficiency of emission to the far field lead to the enhancement of CdSe/ZnS QD monolayer films, which have been proved by previous reports in theory and experiment. [33, 44, 56, 57]

Conclusions

In summary, vertically aligned Au nanorod monolayers with ~7.7 nm edge-to-edge gap size have been prepared by the evaporation-induced self-assembly strategy at the internal region of drying droplet, where a near-equilibrium status is formed. This approach is extended to Au nanorods with the aspect ratio of 2.1, 2.3, 2.7, 2.9 and 3.2, where the longitudinal plasmon bands are 656, 680, 717, 755 and 780 nm, respectively. A vertically aligned Au nanorod bi-layer is formed by decreasing the Debye length to 1.3 nm. During the self-assembly of Au nanorods, the electrostatic force and van der Waals force predominate, determining the self-assembling behavior of Au nanorods. Based on the vertically aligned monolayer consisting of Au nanorods with a longitudinal plasmon band at 717 nm, we investigate the energy transfer between the plasmonic monolayer and CdSe/ZnS QDs. The SiO_2 films deposited by sputtering are used as the spacer to control the distance between the plasmonic array and QDs. The CdSe/ZnS QD monolayer is coated on the vertically aligned Au nanorod monolayer. A maximum enhancement of 10.4 times is achieved at the 20 nm spacer, where the life time of CdSe/ZnS QDs is minimized to 0.9 ns. The PL enhancement is due to three components: the increased excitation transition rate of electrons from valence band to conduction band, the increased radiative rate in the case of exciton recombination for emission, and the increased coupling efficiency of PL to the far field through the scattering of the vertically aligned Au nanorod monolayer.

Acknowledgement:

Q.X. and H.V.D. gratefully acknowledge a strong support from Singapore National Research Foundation via a Competitive Research Program (NRF-CRP- 6-2010-2). Q.X. also thanks the strong support from Singapore National Research Foundation through a fellowship grant (NRF-RF-2009-06), and Singapore Ministry of Education via two Tier2 grants (MOE2011-T2-2-051 and MOE2011-T2-2-085). Additionally, H.V.D thankfully acknowledges Singapore National Research Foundation Fellowship Program (NRF-RF-2009-09).

Notes and references

[a] *Division of Physics and Applied Physics, School of Physical and Mathematical Sciences, Nanyang Technological University, Singapore 637371. Email address: hvdemir@ntu.edu.sg and Qihua@ntu.edu.sg*
[b] *NOVITAS, Nanoelectronics Centre of Excellence, School of Electrical and Electronic Engineering, Nanyang Technological University, Singapore 639798*
[c] *LUMINOUS, Centre of Excellence for Semiconductor Lighting and Displays, School of Electrical and Electronic Engineering, Nanyang Technological University, Singapore 639798*
[d] *Bilkent University, Department of Physics, Department of Electrical and Electronics Engineering, and UNAM – Institute of Materials Science and Nanotechnology, TR-06800, Ankara, Turkey*

1. H. Wang, D. W. Brandl, P. Nordlander and N. J. Halas, *ACC. Chem. Res.*, 2007, **40**, 53-62.
2. M. L. Brongersma and V. M. Shalaev, *Science*, 2010, **328**, 440-441.
3. B. Luk'yanchuk, N. I. Zheludev, S. A. Maier, N. J. Halas, P. Nordlander, H. Giessen and C. T. Chong, *Nat. Mater.* , 2010, **9**, 707-715.
4. Q. Zhang, X. Wen, G. Li, Q. Ruan, J. Wang and Q. Xiong, *ACS Nano*, 2013, DOI: 10.1021/nn4047716.
5. X. L. Xu, B. Peng, D. H. Li, J. Zhang, L. M. Wong, Q. Zhang, S. J. Wang and Q. H. Xiong, *Nano. Lett.*, 2011, **11**, 3232-3238.
6. A. Dong, J. Chen, S. J. Oh, W.-k. Koh, F. Xiu, X. Ye, D.-K. Ko, K. L. Wang, C. R. Kagan and C. B. Murray, *Nano. Lett.*, 2011, **11**, 841-846.
7. A. Tao, P. Sinsermsuksakul and P. Yang, *Nat. Nanotechnol.*, 2007, **2**, 435-440.
8. B. Peng, D. Chen, Z. T. Deng, T. Wen, X. W. Meng, X. L. Ren, J. Ren and F. Q. Tang, *Chemphyschem*, 2010, **11**, 3744-3751.
9. B. Peng, Z. T. Deng, F. Q. Tang, D. Chen, X. L. Ren and J. Ren, *Cryst. Growth. Des.*, 2009, **9**, 4745-4751.
10. W. Cheng, M. J. Campolongo, J. J. Cha, S. J. Tan, C. C. Umbach, D. A. Muller and D. Luo, *Nat. Mater.*, 2009, **8**, 519-525.
11. M. N. Martin, J. I. Basham, P. Chando and S.-K. Eah, *Langmuir*, 2010, **26**, 7410-7417.
12. J. X. Huang, A. R. Tao, S. Connor, R. R. He and P. D. Yang, *Nano. Lett.*, 2006, **6**, 524-529.
13. S. J. Tan, M. J. Campolongo, D. Luo and W. L. Cheng, *Nat. Nanotechnol.*, 2011, **6**, 268-276.
14. P. Yang, *Nature*, 2003, **425**, 243-244.
15. F. Kim, S. Kwan, J. Akana and P. Yang, *J. Am. Chem. Soc.*, 2001, **123**, 4360-4361.
16. K. C. Ng, I. B. Udagedara, I. D. Rukhlenko, Y. Chen, Y. Tang, M. Premaratne and W. Cheng, *ACS Nano*, 2011.
17. T. K. Sau and C. J. Murphy, *Langmuir*, 2005, **21**, 2923-2929.
18. B. Nikoobakht, Z. L. Wang and M. A. El-Sayed, *J. Chem. Phys. B*, 2000, **104**, 8635-8640.
19. T. Ming, X. Kou, H. Chen, T. Wang, H.-L. Tam, K.-W. Cheah, J.-Y. Chen and J. Wang, *Angew. Chem. Int. Ed.* , 2008, **47**, 9685-9690.
20. Y. Xie, S. Guo, Y. Ji, C. Guo, X. Liu, Z. Chen, X. Wu and Q. Liu, *Langmuir*, 2011, **27**, 11394-11400.
21. A. Guerrero-Martínez, J. Pérez-Juste, E. Carbó-Argibay, G. Tardajos and L. M. Liz-Marzán, *Angew. Chem. Int. Ed.* , 2009, **48**, 9484-9488.
22. R. A. Alvarez-Puebla, A. Agarwal, P. Manna, B. P. Khanal, P. Aldeanueva-Potel, E. Carbo-Argibay, N. Pazos-Perez, L. Vigderman, E. R. Zubarev, N. A. Kotov and L. M. Liz-Marzan, *Proc. Natl. Acad. Sci. U. S. A.* , 2011, **108**, 8157-8161.
23. T. Thai, Y. H. Zheng, S. H. Ng, S. Mudie, M. Altissimo and U. Bach, *Angew. Chem. Int. Ed.* , 2012, **51**, 8732-8735.
24. B. Peng, G. Li, D. Li, S. Dodson, Q. Zhang, J. Zhang, Y. H. Lee, H. V. Demir, X. Yi Ling and Q. Xiong, *ACS Nano*, 2013, **7**, 5993-6000.
25. L. Novotny, P. Anger and P. Bharadwaj, *Phys. Rev. Lett.*, 2006, **96**, 113002.
26. B. Peng, Q. Zhang, X. F. Liu, Y. Ji, H. V. Demir, C. H. A. Huan, T. C. Sum and Q. H. Xiong, *ACS Nano*, 2012, **6**, 6250-6259.

27. T. Pons, I. L. Medintz, K. E. Sapsford, S. Higashiya, A. F. Grimes, D. S. English and H. Mattoussi, *Nano. Lett.*, 2007, **7**, 3157-3164.
28. G. Schneider, G. Decher, N. Nerambourg, R. Praho, M. H. V. Werts and M. Blanchard-Desce, *Nano. Lett.*, 2006, **6**, 530-536.
29. K. Munechika, Y. C. Chen, A. F. Tillack, A. P. Kulkarni, I. Jen-La Plante, A. M. Munro and D. S. Ginger, *Nano. Lett.*, 2011, **11**, 2725-2730.
30. Q. Zhang, X. Y. Shan, X. Feng, C. X. Wang, Q. Q. Wang, J. F. Jia and Q. K. Xue, *Nano. Lett.*, 2011, **11**, 4270-4274.
31. S. Kühn, U. Håkanson, L. Rogobete and V. Sandoghdar, *Phys. Rev. Lett.*, 2006, **97**, 017402.
32. K. Munechika, Y. Chen, A. F. Tillack, A. P. Kulkarni, I. J. L. Plante, A. M. Munro and D. S. Ginger, *Nano. Lett.*, 2010, **10**, 2598-2603.
33. Y. K. Wang, T. Y. Yang, M. T. Tuominen and M. Achermann, *Phys. Rev. Lett.*, 2009, **102**, 163001.
34. P. F. Guo, S. Wu, Q. J. Ren, J. Lu, Z. H. Chen, S. J. Xiao and Y. Y. Zhu, *J. Phys. Chem. Lett.*, 2010, **1**, 315-318.
35. O. Kulakovich, N. Strekal, A. Yaroshevich, S. Maskevich, S. Gaponenko, I. Nabiev, U. Woggon and M. Artemyev, *Nano. Lett.*, 2002, **2**, 1449-1452.
36. X. Wen, G. Li, J. Zhang, Q. Zhang, B. Peng, L. M. Wong, S. Wang and Q. Xiong, *Nanoscale*, 2014, DOI: 10.1039/C3NR04012G.
37. C. Cao, J. Zhang, X. Wen, S. L. Dodson, N. T. Dao, L. M. Wong, S. Wang, S. Li, A. T. Phan and Q. Xiong, *ACS Nano*, 2013, **7**, 7583-7591.
38. J. X. Fang, S. Y. Du, S. Lebedkin, Z. Y. Li, R. Kruk, M. Kappes and H. Hahn, *Nano. Lett.*, 2010, **10**, 5006-5013.
39. T. Ming, L. Zhao, Z. Yang, H. Chen, L. Sun, J. Wang and C. Yan, *Nano. Lett.*, 2009, **9**, 3896-3903.
40. K. L. Young, M. R. Jones, J. Zhang, R. J. Macfarlane, R. Esquivel-Sirvent, R. J. Nap, J. S. Wu, G. C. Schatz, B. Lee and C. A. Mirkin, *Proc. Natl. Acad. Sci. U. S. A.*, 2012, **109**, 2240-2245.
41. K. J. M. Bishop, C. E. Wilmer, S. Soh and B. A. Grzybowski, *Small*, 2009, **5**, 1600-1630.
42. H. Ohshima and A. Hyono, *J. Colloid. Interface. Sci.*, 2009, **333**, 202-208.
43. A. M. Funston, C. Novo, T. J. Davis and P. Mulvaney, *Nano Lett.*, 2009, **9**, 1651-1658.
44. F. Tam, G. P. Goodrich, B. R. Johnson and N. J. Halas, *Nano. Lett.*, 2007, **7**, 496-501.
45. J. R. Lakowicz, K. Ray and R. Badugu, *Langmuir*, 2006, **22**, 8374-8378.
46. K. T. Shimizu, W. K. Woo, B. R. Fisher, H. J. Eisler and M. G. Bawendi, *Phys. Rev. Lett.*, 2002, **89**, 117401.
47. R.-M. Ma, R. F. Oulton, V. J. Sorger, G. Bartal and X. Zhang, *Nat. Mater.*, 2011, **10**, 110-113.
48. R. Carminati, J. J. Greffet, C. Henkel and J. M. Vigoureux, *Opt. Commun.*, 2006, **261**, 368-375.
49. L. Novotny, *J. Opt. Soc. Am. A.*, 1997, **14**, 91-104.
50. L. Novotny and B. Hecht, *Principles of Nano-Optics. In Dipole Emission Near Planar Interfaces*, Cambridge University Press, 2007, 335-346.
51. A. O. Govorov, G. W. Bryant, W. Zhang, T. Skeini, J. Lee, N. A. Kotov, J. M. Slocik and R. R. Naik, *Nano. Lett.*, 2006, **6**, 984-994.
52. X. L. Xu, Y. Y. Zhao, E. J. Sie, Y. H. Lu, B. Liu, S. A. Ekahana, X. Ju, Q. K. Jiang, J. B. Wang, H. D. Sun, T. C. Sum, C. H. A. Huan, Y. P. Feng and Q. H. Xiong, *ACS Nano*, 2011, **5**, 3660-3669.
53. A. F. van Driel, I. S. Nikolaev, P. Vergeer, P. Lodahl, D. Vanmaekelbergh and W. L. Vos, *Phys. Rev. B*, 2007, **75**, 035329.
54. G. W. Shu, W. Z. Lee, I. J. Shu, J. L. Shen, J. C. A. Lin, W. H. Chang, R. C. Ruaan and W. C. Chou, *IEEE. T. Nanotechnol.*, 2005, **4**, 632-636.
55. W. Z. Lee, G. W. Shu, J. S. Wang, J. L. Shen, C. A. Lin, W. H. Chang, R. C. Ruaan, W. C. Chou, C. H. Lu and Y. C. Lee, *Nanotechnology*, 2005, **16**, 1517-1521.
56. O. G. Tovmachenko, C. Graf, D. J. van den Heuvel, A. van Blaaderen and H. C. Gerritsen, *Adv. Mater.*, 2006, **18**, 91-95.
57. Y. H. Chan, J. X. Chen, S. E. Wark, S. L. Skiles, D. H. Son and J. D. Batteas, *ACS Nano*, 2009, **3**, 1735-1744.

TOC

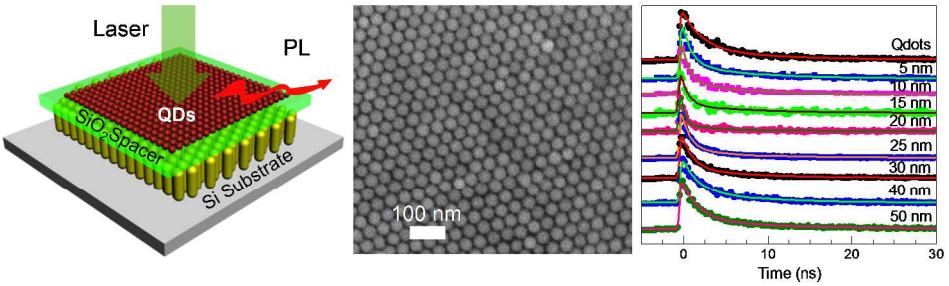

A vertically aligned CTAB-coated Au nanorod monolayer was formed by the evaporation-induced self-assembly, which provides a unique anisotropic plasmonic system to investigate the energy transfer between the plasmonic array and fluorophores.